

Learning-based Robust Speaker Counting and Separation with the Aid of Spatial Coherence

Yicheng Hsu¹ and Mingsian R. Bai^{1,2*}

Abstract

A two-stage approach is proposed for speaker counting and speech separation in noisy and reverberant environments. A spatial coherence matrix (SCM) is computed using whitened relative transfer functions (wRTFs) across time frames. The global activity functions of each speaker are estimated on the basis of a simplex constructed using the eigenvectors of the SCM, while the local coherence functions are computed from the coherence between the wRTFs of a time-frequency bin and the global activity function-weighted RTF of the target speaker. In speaker counting, we use the eigenvalues of the SCM and the maximum similarity of the interframe global activity distributions between two speakers as the input features to the speaker counting network (SCnet). In speaker separation, a global and local activity-driven network (GLADnet) is utilized to estimate a speaker mask, which is particularly useful for highly overlapping speech signals. Experimental results obtained from the real meeting recordings demonstrated the superior speaker counting and speaker separation performance achieved by the proposed learning-based system without prior knowledge of the array configurations.

Keywords: multichannel blind source separation, speaker counting and separation, spatial coherence, neural network

1 Introduction

Blind source separation (BSS) involves extracting individual speech sources from a mixture signal with no prior knowledge of the speakers and mixing systems [1]. BSS finds application in smart voice assistants, hands-free teleconferencing, automatic meeting transcription, etc., where only mixture signals received by a single or multiple microphones are available. Various BSS algorithms have been developed based on different assumptions of the characteristics of the speech sources and the mixing systems [2]–[9]. Learning-based BSS approaches have recently received increased research attention due to the advances of the deep learning hardware and software. Promising results have been obtained using single-channel neural networks (NNs) [10]–[15]. To further improve separation performance, techniques that leveraged spatial information embedded in microphone array signals began to emerge [16]–[19]. The number of speakers must be known before applying

these BSS techniques. As a key step prior to speaker separation, speaker counting [20] will be examined next.

In some studies, the maximum number of speakers was always assumed during speaker separation [21]–[24]. However, the choice of the number was critical. Another approach was to extract speech signals in a recursive manner [25, 26], where the BSS problem was tackled by a multi-pass source-extraction procedure based on a recurrent neural network (RNN). However, the convergence criterion was difficult to set, and distortions would accumulate with iteration. To address the distortion problem, a coarse-to-fine recursive speech separation method was proposed in [27]. Unlike the previous methods which conducted implicit speaker counting into separation, a multi-decoder DPRNN [28] employed a count-head to infer the number of speakers and multiple decoder heads to separate the signals. A speaker counting technique was suggested using a scheme that alternated between speech enhancement and speaker separation [29].

*Correspondence: msbai@pme.nthu.edu.tw

In real-world applications, separation performance can be degraded by room reverberation and background noise. Under such circumstances, multichannel approaches can be more advantageous than the mono-channel approaches. For example, deep clustering-based speaker counting and mask estimation were incorporated into masking-based linear beamforming for speaker separation tasks [30]. Chazan et al. presented the use of a deep-neural-network (DNN)-based single-microphone concurrent speaker detector for source counting, followed by beamformer coefficient estimation for speaker separation [31, 32].

Despite the promising results obtained using DNN-based approaches, have shown, most network models require a large amount of data for training. Another limitation is that identical array configurations used in the testing phase and the training phase are preferable. Therefore, data-driven approaches may have certain advantages. Laufer-Goldshtein *et al.* proposed the global and local simplex separation algorithm by exploiting the correlation matrix of relative transfer functions (RTFs) across time frames [33]. The number of speakers is determined from the eigenvalue decay of the correlation matrix. The activity probabilities of each speaker were estimated from the simplex formed by eigenvectors. In the separation stage, a spectral mask was computed for the identified dominant speakers, followed by spatial beamforming and post-filtering. Although the simplex-based approach was very effective in most cases, it does not work well for low-activity speakers [34].

Instead of exhaustive separation, one may selectively extract only the target speech signal, with the aid of auxiliary information such as video images [35, 36], pre-enrolled utterances [37]–[39], and the location of the target speaker [40]–[43]. Although the target speaker extraction approach results in significant performance improvements, the auxiliary information may not always be accessible. To overcome this issue, the speaker activity-driven speech extraction neural network [44] was proposed to facilitate target speaker extraction by

monitoring speaker activities. However, the speaker activity-driven speech extraction neural network is prone to adverse acoustic conditions in speaker extraction with speaker activity information alone.

Inspired by Gannot et al. [33, 45], we propose a learning-based speaker counting and an activity-driven speaker separation algorithm in this paper. However, as differing from their approach, we compute a modified coherence matrix using whitened relative transfer functions (wRTFs) across time frames. In the speaker counting stage, we use the eigenvalues of the spatial coherence matrix and the maximum similarity between the global activity distribution of two speakers across time frames as the input features for the speaker counting network (SCnet). In the separation stage, the local coherence functions of the target speaker are generated by using the coherence between the wRTF of each time-frequency (TF) bin and the wRTF weighted by the corresponding global activity function. Next, a global and local activity-driven network (GLADnet) is used to estimate a target mask. As will be shown, the proposed GLADnet proves to be effective, even for “mismatched” room impulse responses (RIRs) and array configurations (including array geometry and inter-element spacing) that differ from those used in the training phase.

We train our DNN models with RIRs simulated using the image-source method [46], whereas the trained models are tested using the measured RIRs recorded at Bar-Ilan University [47]. Real-life recordings from the LibriCSS meeting corpus [48] are also adopted to validate the proposed separation networks. In this paper, the proposed speaker counting and speaker separation algorithm are compared with the simplex-based methods developed by Laufer-Goldshtein *et al.* [33] in terms of F1 scores and confusion matrices. Perceptual evaluation of speech quality (PESQ) [49] and word error rate (WER) are adopted as the performance measures in speaker separation tasks.

While inspired by Ref. [33], this study presents three key contributions distinct from the prior work. First, a

learning-based robust speaker counting and activity-driven speaker separation algorithm is developed. Second, a modified spatial coherence matrix is formulated to effectively capture the spatial information of independent speakers. A novel idea based on maximum similarity between the global activity distribution of two speakers over time frames is explored to serve as the input feature to speaker counting. Third, an array configuration-agnostic GLADnet informed by the global and local activities of speakers is suggested.

The remainder of this paper is organized as follows. Section II discusses the previous work related to our approach. Section III gives the problem formulation and a brief review of the simplex-based approach, which is used as the baseline in this study. Section IV presents the proposed speaker counting and speaker separation system. The proposed system is compared with several baselines in Section V through extensive experiments. Section VI concludes this paper.

2 Problem formulation and the baseline approach

2.1 Problem formulation

Consider a scenario in which utterances of J speakers are captured using M distant microphones in a reverberant room. We assume that no prior knowledge of the array configuration is available. The array signal model is described in the short-time Fourier transform (STFT) domain. The received signal at the m th microphone can be written as

$$X^m(l, f) = \sum_{j=1}^J A_j^m(f) S_j(l, f) + V^m(l, f), \quad (1)$$

where l and f denote the time frame index and frequency bin index, respectively, $A_j^m(f)$ denotes the acoustic transfer function between the m th microphone and the j th speaker, $S_j(l, f)$ denotes the signal of the j th speaker, and $V^m(l, f)$ denotes the additive sensor noise. The goal of this study is to estimate the number of speakers J (speaker counting) and extract independent speaker signals from the microphone mixture signals with no

information regarding the sources and the mixing process.

2.2 Baseline method: the simplex-based approach

The simplex-based approach [33, 34] is based on the global and local simplex representations and relies on the assumption of the speech sparsity in the STFT domain [50]. By assuming speech sparsity, each TF bin is dominated by either the speaker or the noise. The ideal indicator selected in each TF bin can be expressed as

$$I_j(l, f) = \begin{cases} 1 & j\text{th speaker is dominant} \\ 0 & \text{otherwise} \end{cases} \quad (2)$$

If a TF bin is not dominated by any speakers, such a TF bin will be dominated by noise, i.e., $\sum_{j=1}^J I_j(l, f) = 0$.

Let $p_j^G(l)$ be the probability of speaker j in frame l :

$$p_j^G(l) = \frac{1}{F} \sum_{f=1}^F I_j(l, f) \quad (3)$$

which is the global probability associated with the j th speaker. Note that the probabilities $\{p_j^G(l)\}_{j=1}^J$ depend only on the frame index, not on the frequency index.

2.2.1 Feature extraction

On the speech sparsity assumption in the TF domain, the relative transfer function (RTF) [51] associated with the j th speaker of the m th microphone signal with respect to the first (reference) microphone signal can be written as

$$R^m(l, k) = \frac{X^m(l, k)}{X^1(l, k)} = \begin{cases} \frac{A_j^m(f)}{A_j^1(f)} & \text{for } I_j(l, f) = 1, 1 \leq j \leq J \\ \frac{V^m(l, f)}{V^1(l, f)} & \text{for } \sum_{j=1}^J I_j(l, f) = 0 \end{cases} \quad (4)$$

In the following, a feature vector $\mathbf{r}(l)$ for each frame l is defined to compose $D = 2 \times (M-1) \times K$ elements of the real and imaginary parts of the computed ratios (4) for $1 \leq k \leq K$ frequency bins and in $(M-1)$ microphone signals:

$$\begin{aligned}
\mathbf{r}^m(l) &= [R^m(l, f_1) \ R^m(l, f_2) \ \cdots \ R^m(l, f_K)] \\
\mathbf{r}^c(l) &= [\mathbf{r}^2(l) \ \mathbf{r}^3(l) \ \cdots \ \mathbf{r}^M(l)] \\
\mathbf{r}(l) &= [\text{real}\{\mathbf{r}^c(l)\} \ \text{imag}\{\mathbf{r}^c(l)\}]^T
\end{aligned} \tag{5}$$

where $\{f_k\}_{k=1}^K$, are the selected frequencies. The correlation matrix $\mathbf{W} \in \mathbb{R}^{L \times L}$ is computed, where $[\mathbf{W}]_{lm} = \frac{1}{D} \mathbf{r}^T(l) \mathbf{r}(m)$. \mathbf{W} can be approximated as [45]

$$\mathbf{W} \approx \mathbf{P} \mathbf{P}^T \tag{6}$$

where $\mathbf{P} = [\mathbf{p}_1^G \ \cdots \ \mathbf{p}_J^G] \in \mathbb{R}^{L \times J}$ is composed of the global probabilities $\mathbf{p}_j^G \in \mathbb{R}^{L \times 1}$ associated with each speaker.

2.2.2 Speaker counting

For J independent speakers, the matrix \mathbf{P} should have rank J . It follows that the number of speakers can be determined by counting the principal eigenvalues of the correlation matrix \mathbf{W} . However, selecting an appropriate threshold is not straightforward because of complex acoustic conditions. To select a proper threshold, the speaker counting problem was formulated as a classification problem [33], where each class corresponds to a different number of speakers. A feature vector consisting of the first principal J' eigenvalues of the correlation matrix serve as the input to the classifier

$$\mathbf{f}_{\text{baseline } 1} = [\lambda_1 \ \lambda_2 \ \cdots \ \lambda_{J'}]^T \tag{7}$$

where J' is the maximally possible number of speakers and is set to 4 in this study. The multiclass support vector machine (SVM) was used as the classifier in [33].

2.2.3 Speaker separation

Once the number of speakers (J) is available, the eigenvectors associated with the J largest eigenvalues for each frame l are selected to form the global mapping vector

$$\mathbf{v}^G(l) = [u_1(l), u_2(l), \dots, u_J(l)]^T \tag{8}$$

According to [33, 45], the global mapping vector $\mathbf{v}^G(l)$ can be expressed as a linear transformation of the global probability vector $\mathbf{p}^G(l)$:

$$\mathbf{v}^G(l) = \mathbf{G} \mathbf{p}^G(l) \tag{9}$$

with embedded information of speaker activities. The successive projection algorithm [52] can be applied to identify the simplex vertices and construct the transformation matrix $\mathbf{G} = [\mathbf{v}^G(l_1), \mathbf{v}^G(l_2), \dots, \mathbf{v}^G(l_J)]$, where $\{l_j\}_{j=1}^J$ represent frame indices of the simplex vertices. Hence, the global probability can be computed.

$$\mathbf{p}^G(l) = [p_1^G(l), p_2^G(l), \dots, p_J^G(l)]^T = \mathbf{G}^{-1} \mathbf{v}^G(l) \tag{10}$$

For the local mapping, each TF bin is assigned to a dominant speaker or noise. The spectral mask can be obtained by using the weighted nearest-neighbor rule.

$$M(l, f) = \arg \max_{j \in \{1, \dots, J+1\}} \frac{1}{\pi_j} \sum_{n=1}^L \omega_n(f) p_j^G(n) \tag{11}$$

where $\pi_j = \sum_{n=1}^L p_j^G(n)$ denotes the class normalization factor and $\omega_n(f)$ is a Gaussian weighting function [34]:

$$\omega_n(f) = \exp\{-\|\mathbf{r}(l, f) - \mathbf{r}(n, f)\|\} \tag{12}$$

that is inversely related to the distance in the space defined by the local representation $\{\mathbf{r}(l, f)\}_{l=1}^L$ between frame n and frame l . The signal of the j th speaker can be estimated by applying the spectral mask in (11) to the reference microphone signal:

$$\hat{S}_j^{\text{Mask}}(l, f) = \begin{cases} X^1(l, f) & \text{if } M(l, f) = j \\ \beta X^1(l, f) & \text{otherwise,} \end{cases} \tag{13}$$

where β is the attenuation factor to avoid musical noise. In this paper, β is set to 0.1 as in [33].

A linearly constrained minimum variance (LCMV) beamformer can be used to extract each independent speaker signals [33, 34], with the weights below

$$\mathbf{w}_{LCMV} = \mathbf{R}_m^{-1}(f) \hat{\mathbf{A}}(f) \left(\hat{\mathbf{A}}^H(f) \mathbf{R}_m^{-1}(f) \hat{\mathbf{A}}(f) \right)^{-1} \mathbf{g}_j, \tag{14}$$

where $\hat{\mathbf{A}}(f) = [\hat{\mathbf{a}}_1(f), \dots, \hat{\mathbf{a}}_J(f)]^T \in \mathbb{C}^{M \times J}$ denotes the

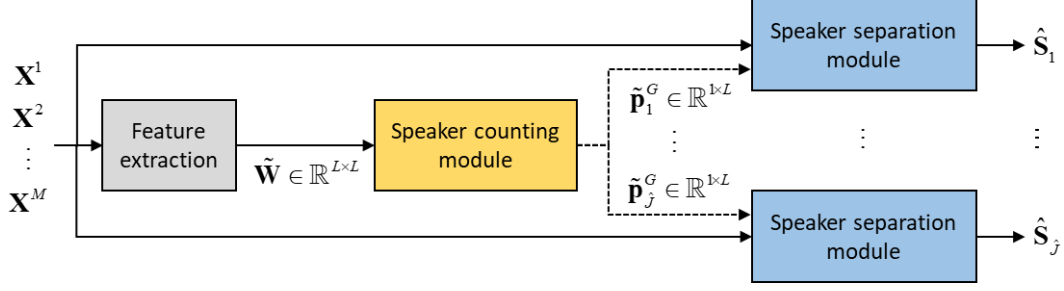


Figure 1 Block diagram of the proposed speaker counting and separation system.

RTF matrix with $\hat{\mathbf{a}}_j(f) = [\hat{A}_j^1(f), \hat{A}_j^2(f), \dots, \hat{A}_j^M(f)]^T$ of the j th speaker and $\mathbf{R}_{nm}(f)$ is the noise covariance matrix. In this study, only sensor noise is assumed, i.e., $\mathbf{R}_{nm} = \sigma_{nm} \mathbf{I}$. As a result, (14) reduces to

$$\mathbf{w}_{LCMV} = \hat{\mathbf{A}}(f) (\hat{\mathbf{A}}^H(f) \hat{\mathbf{A}}(f))^{-1} \mathbf{g}_j \quad (15)$$

where the RTF of the j th speaker can be estimated by

$$\hat{A}_j^m(f) = \frac{\sum_{l \in \mathcal{L}_j} X^m(l, f) X^{1*}(l, f)}{\sum_{l \in \mathcal{L}_j} X^1(l, f) X^{1*}(l, f)} \quad (16)$$

where $\mathcal{L}_j = \{l | p_j^G(l) > \varepsilon, l \in \{1, \dots, L\}\}$ denotes the set of frames dominated by the j th speaker, and $\varepsilon = 0.2$ is a probability threshold.

To further illuminate the residual noise and interference, a single-channel mask is applied [33, 34], as given by

$$\hat{S}_j^{LCMV-Mask}(l, f) = \begin{cases} \mathbf{w}_{LCMV}^H \mathbf{x}(l, f) & \text{if } M(l, f) = j \\ \beta \mathbf{w}_{LCMV}^H \mathbf{x}(l, f) & \text{otherwise,} \end{cases} \quad (17)$$

where the vector $\mathbf{x}(l, f) = [X^1(l, f), \dots, X^M(l, f)]^T$ denotes the microphone signals and $\beta = 0.2$ is a small factor to prevent from musical noise.

3 Proposed method

Inspired by the above-mentioned simplex-based approach, we develop a robust speaker counting and separation system by exploiting spatial coherence features of array signals, as illustrated in Figure 1. The system consists of three modules: the feature-extraction module (Section III-A), the speaker counting module

(Section III-B), and the speaker separation module (Section III-C), as detailed in the sequel.

3.1 Spatial feature extraction

Instead of the real feature vector used in the simplex-based approach, a “whitened” complex feature vector $\tilde{\mathbf{r}}(l)$ is defined as

$$\tilde{\mathbf{r}}(l) = [\tilde{\mathbf{r}}(l, f_1) \ \tilde{\mathbf{r}}(l, f_2) \ \dots \ \tilde{\mathbf{r}}(l, f_K)]^T \in \mathbb{C}^{(M-1)K \times 1} \quad (18)$$

where

$$\tilde{\mathbf{r}}(l, f) = \begin{bmatrix} R^2(l, f) & \dots & R^M(l, f) \\ \overline{R^2(l, f)} & \dots & \overline{R^M(l, f)} \end{bmatrix}$$

$R^m(l, f)$ is defined in (4), and $\{f_k\}_{k=1}^K$ is the selected frequency band as in (5). Next, we construct a spatial coherence matrix $\tilde{\mathbf{W}} \in \mathbb{R}^{L \times L}$ with the ln th entry defined as

$$\tilde{W}_{ln} = \frac{\text{Re}\{\tilde{\mathbf{r}}^H(l) \tilde{\mathbf{r}}(n)\}}{\|\tilde{\mathbf{r}}(l)\| \|\tilde{\mathbf{r}}(n)\|} = \frac{1}{\tilde{D}} \text{Re}\{\tilde{\mathbf{r}}^H(l) \tilde{\mathbf{r}}(n)\} \quad (19)$$

where $\text{Re}\{\cdot\}$ is the real-part operator, $\|\cdot\|$ denotes the l_2 -norm, and $\tilde{D} = \|\tilde{\mathbf{r}}(l)\| \|\tilde{\mathbf{r}}(n)\| = (M-1)K$ due to the fact that the feature vectors have been whitened. Note that the complex inner product of $\tilde{\mathbf{r}}(l)$ and $\tilde{\mathbf{r}}(n)$ is computed, which can also be regarded as a sign-sensitive cosine similarity based on the Euclidean angle [53]. An example of the spatial correlation matrix computed using the method reported in the references [33, 34, 45] and the proposed spatial coherence matrix are compared in Fig. 2, which is generated using a 12-second clip with a three-speaker mixture speaker mixture captured by an eight-

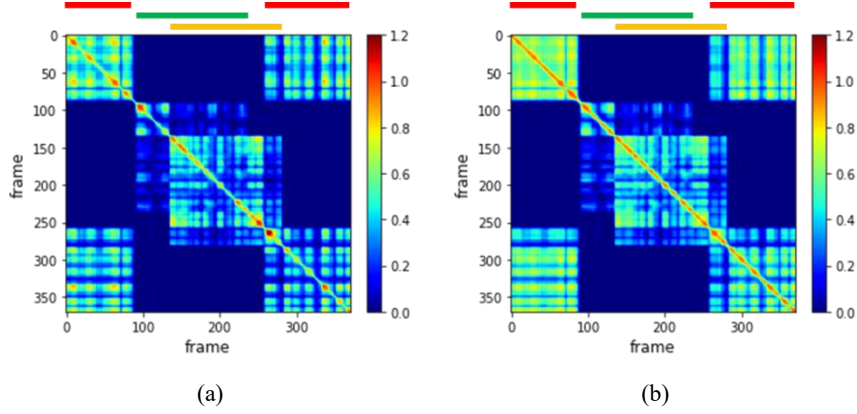


Figure 2 Examples of (a) the spatial correlation matrix \mathbf{W} and (b) the spatial coherence matrix $\tilde{\mathbf{W}}$. The color bars on the top of each figure denote the active period of each speaker.

element uniform linear array (ULA) with interelement spacing of 8 cm. The proposed matrix shows more salient speaker activity features than the former spatial correlation matrix. In addition, the range of the proposed coherence matrix is within $[-1, 1]$, which is a desired property for network training.

3.2 Speaker counting

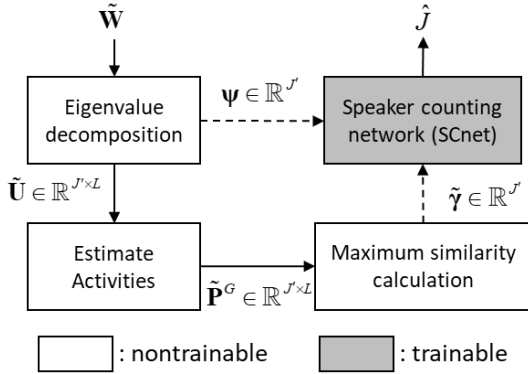


Figure 3 Flowchart of the proposed speaker counting approach.

The flowchart of the proposed speaker counting approach is detailed in Fig. 3. Two features related to the speaker count are extracted from the spatial coherence matrix $\tilde{\mathbf{W}}$ and input to the speaker counting network (SCnet), as will be detailed next.

In this study, we propose to use the eigenvalues

$\{\tilde{\lambda}_n\}_{n=1}^L$ of the spatial coherence matrix $\tilde{\mathbf{W}}$ as the feature for the classifier. An example of scatter pattern of the eigenvalues to discriminate between different speaker count classes, $J \in \{1, 2, 3, 4\}$, is illustrated in Fig. 4. We generated 2000-sample speech mixtures for 1-4 speakers, with 0%, 10%, 20%, 30%, 40% overlap ratios. Sensor noise was added with 10 dB SNR. Dry signals were convoluted with the measured RIRs selected from the Multi-Channel Impulse Responses Database [47] that was recorded using an eight-element ULA with interelement spacing of 8 cm and $T_{60} = 0.61$ s. Each cross in the figure represents one observation to specify the number of speakers. Figure 3 demonstrates the ability of the eigenvalues obtained from the correlation matrix and the coherence matrix to discriminate between different numbers of speakers. In addition, the eigenvalues of the coherence matrix $\tilde{\mathbf{W}}$ can discriminate between different numbers of speakers better than those of the correlation matrix \mathbf{W} . However, some of the observations cannot be classified into the correct class according to the eigenvalues.

Apart from eigenvalues of the spatial coherence matrix, another feature that can help speaker counting is introduced to deal with meeting scenarios in which the overlap ratio of conversation is often less than 20% [54].

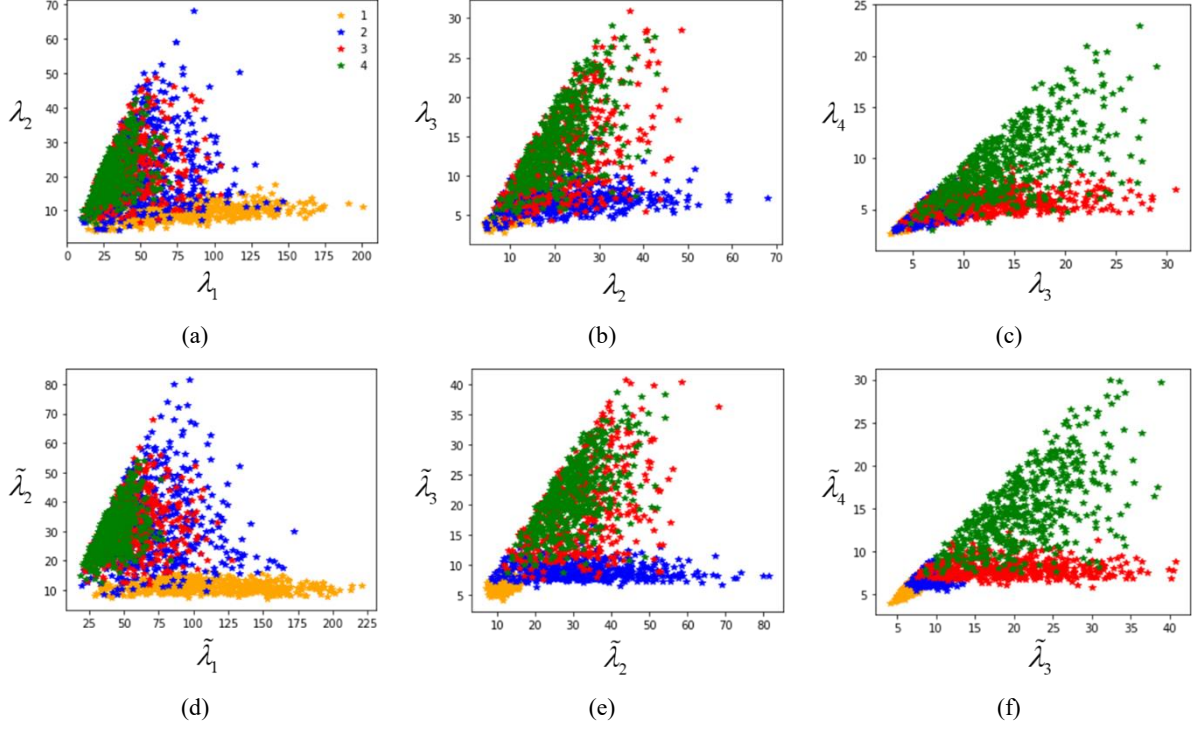


Figure 4 Scatter plots of the eigenvalues corresponding to the observations with $J \in \{1, 2, 3, 4\}$ speakers. Each cross with different color represents an observation corresponding to different number of speakers.

For such scenarios, we first calculate a similarity matrix $\tilde{\gamma}^J \in \mathbb{R}^{\tilde{J} \times \tilde{J}}$ of \tilde{J} speakers with the pq -th entry defined as

$$\tilde{\gamma}_{pq}^J = \frac{\tilde{\mathbf{p}}_p^G \cdot \tilde{\mathbf{p}}_q^G}{\|\tilde{\mathbf{p}}_p^G\| \|\tilde{\mathbf{p}}_q^G\|} \quad (20)$$

where “ \cdot ” denotes the inner product, $\tilde{\mathbf{p}}_p^G \in \mathbb{R}^{L \times 1}$ and $\tilde{\mathbf{p}}_q^G \in \mathbb{R}^{L \times 1}$ denote the global probabilities of the p th and the q th speakers estimated from the spatial coherence matrix $\tilde{\mathbf{W}}$, and $1 \leq p, q \leq \tilde{J}$. Next, we find the maximum similarity value of all entries but the diagonal entries.

$$\tilde{\gamma}_{\max}^J = \max_{p,q} \left(\tilde{\gamma}_{pq}^J - \mathbf{I} \right)_{pq} \quad (21)$$

Similarly, γ_{\max}^J denotes the maximum similarity calculated using the global probability obtained from the spatial correlation matrix \mathbf{W} . An example of scatter pattern of the maximum similarity to discriminate between different speaker count classes, $J \in \{1, 2, 3, 4\}$, is illustrated in Fig. 5. The data

generation is identical to those of Fig. 4. To visualize the separability by using the proposed feature, we plot the scatter diagram by the projection onto a two-dimensional feature space. Figure 5 suggests that observations are separable via the maximum similarity, which helps to classify the number of speakers. In Fig. 5(a), the single-speaker observations and the two to four speaker observations are clearly separable along the γ_{\max}^2 coordinate. The one or two speaker observations and the three or four speaker observations are clearly separable along the γ_{\max}^3 coordinate. In Fig. 5(b), the one to three speaker observations and the four speaker observations are clearly separable along the γ_{\max}^4 coordinate.

In this study, the speaker counting problem is formulated as a classification problem as in Ref. [33] with four classes corresponding to 1 to 4 speakers. For each observation, the target speaker is indicated by a one-hot vector $\mathbf{z} \in \mathbb{R}^{4 \times 1}$. For inference, the prediction is the highest probability of the output distribution. Three different input feature vectors are defined for the

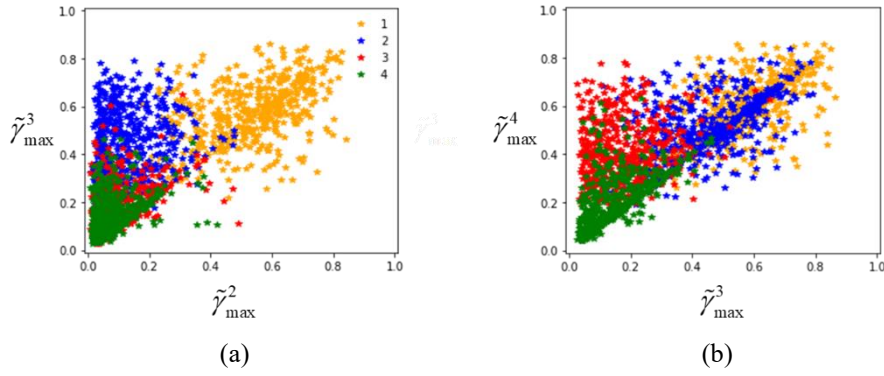


Figure 5 Scatter plots of the maximum similarity to the observations with $J \in \{1, 2, 3, 4\}$ speakers. Each cross with different color represents an observation corresponding to different number of speakers.

assessment of speaker counting performance:

$$\begin{aligned}
 \mathbf{f}_{\text{baseline 2}} &= \begin{bmatrix} \lambda_2 & \dots & \lambda_{J'} \\ \lambda_1 & & \lambda_1 \end{bmatrix}^T \in \mathbb{R}^{J'-1} \\
 \mathbf{f}_{\text{proposal 1}} &= \begin{bmatrix} \tilde{\lambda}_2 & \dots & \tilde{\lambda}_{J'} \\ \tilde{\lambda}_1 & & \tilde{\lambda}_1 \end{bmatrix}^T \in \mathbb{R}^{J'-1} \\
 \mathbf{f}_{\text{proposal 2}} &= \begin{bmatrix} \tilde{\lambda}_2 & \dots & \tilde{\lambda}_{J'} & \tilde{\gamma}_{\max}^2 & \dots & \tilde{\gamma}_{\max}^{J'} \end{bmatrix}^T \in \mathbb{R}^{2(J'-1)},
 \end{aligned} \quad (22)$$

where the eigenvalues are normalized by the maximum eigenvalue for improved convergence. Features $\mathbf{f}_{\text{baseline 2}}$ is obtained from the spatial correlation matrix \mathbf{W} , whereas features $\mathbf{f}_{\text{proposal 1}}$ and $\mathbf{f}_{\text{proposal 2}}$ are obtained from the proposed spatial coherence matrix $\tilde{\mathbf{W}}$.

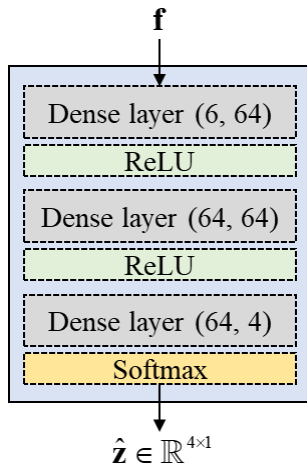


Figure 6 Speaker counting network (SCNet).

A DNN model termed SCnet is used as the classifier for speaker counting. Figure 6 depicts SCnet that is

comprised of three dense layers, followed by a rectified linear unit (ReLU) activation, whereas the softmax activation is adopted in the output layer. The cross-entropy is adopted as the loss function in network training.

3.2 Speaker separation

In contrast to the speaker separation approach presented in II-B, the proposed separation approach is based on the activities of the independent speakers, as shown in Fig. 7. The proposed system primarily consists of two modules: 1) the local coherence estimation of independent speakers, which monitors the local activity of each speaker according to the global probability of the speaker, and 2) the global and local activity-driven network (GLADnet) which extracts the speaker signal with the auxiliary information on the global and local activities of the speaker.

In the local coherence estimation of a speaker, the local coherence is calculated between the wRTF of the target speaker and the wRTF of each TF bin. The wRTF of the j th speaker is calculated as

$$\tilde{\mathbf{a}}_j(f) = \begin{bmatrix} \hat{A}_j^2(f) & \dots & \hat{A}_j^M(f) \\ |\hat{A}_j^2(f)| & \dots & |\hat{A}_j^M(f)| \end{bmatrix}^T \quad (23)$$

where $\hat{A}_j^m(f)$ is the estimated RTF. Thus, the local coherence of the j th speaker is can be calculated.

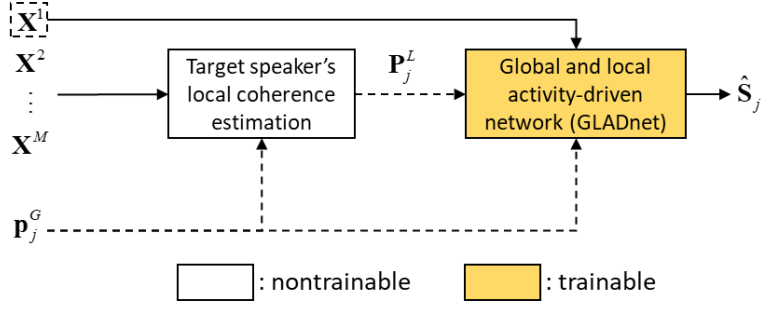


Figure 7 Block diagram of the proposed speaker separation module.

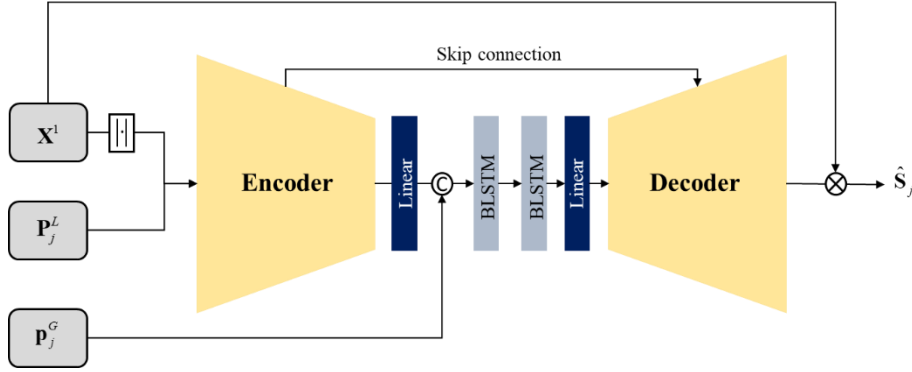


Figure 8 The GLADnet.

$$\begin{aligned}
 p_j^L(l, f) &= \frac{\text{Re}\{\tilde{\mathbf{a}}_j^H(l)\tilde{\mathbf{r}}(l, f)\}}{\|\tilde{\mathbf{a}}_j(l)\|\|\tilde{\mathbf{r}}(l, f)\|} \\
 &= \frac{1}{M-1} \text{Re}\{\tilde{\mathbf{a}}_j^H(l)\tilde{\mathbf{r}}(l, f)\}.
 \end{aligned} \tag{24}$$

Local coherence serves to inform the DNN about the local activity of a speaker.

GLADnet is based on a convolutional recurrent network [55], as illustrated in Fig. 8. The network has three inputs: the magnitude spectrogram of the reference microphone signal, the global activity of the speaker, and the local activity of the speaker. GLADnet has six symmetric encoder and decoder layers with an 8-16-32-128-128-128 filter. The convolutional blocks feature a separable convolution layer, followed by batch normalization, and exponential linear unit activation. The output layer terminates with sigmoid activation. The convolution kernel and step size are set to (3,2) and (2,1), respectively. Note that 1×1 pathway convolutions (PConv) are used as skip connections, which leads to considerable parameter reduction with little performance degradation. The global activity is repeatedly

concatenated to the output of the linear layer with 256 nodes in each time frame. The resulting vector is then fed to the following bidirectional long short-term memory layers with 256 nodes to sift out the latent features pertaining to each speaker. The soft mask estimated by the network is multiplied element-wise with the noisy magnitude spectrogram to yield an enhanced spectrogram. The complete complex spectrogram can be obtained by combining the enhanced magnitude spectrogram with the phase of the noisy spectrogram. The network is trained to minimize the compressed mean square error between the masked magnitude ($\hat{\mathbf{S}}$) and the ground-truth magnitude (\mathbf{S})

$$J_{CMSE} = \sum_{t,f} \left\| |\mathbf{S}|^c - |\hat{\mathbf{S}}|^c \right\|_F^2 \tag{25}$$

where $c = 0.3$ is the compression factor and $\|\cdot\|_F$ denotes the Frobenius norm.

4 Experimental study

Experiments were undertaken to validate the proposed

learning-based speaker counting and separation system. The networks were trained using the simulated RIRs and tested using the measured RIRs with different T60s and array configurations recorded at Bar-Ilan University [47]. For meeting scenarios, we also tested the proposed system on real meeting recordings from the LibriCSS meeting corpus [48].

4.1 Training and validation dataset

In total, 50,000 and 5000 samples were used in training and validation, respectively. Dry speech signals selected from the *train-clean-360* subset of the LibriSpeech corpus [56] were for training and validation. Noisy speech mixtures edited in 12-s clips were prepared with different numbers of speakers $J \in \{1, 2, 3, 4\}$ in reverberation conditions and signal-to-noise ratios (SNRs) between -5 dB and 5 dB. The overlap ratio of the speech mixtures varied from 0% to 40%. Reverberant microphone signals were simulated by filtering the dry signals with the simulated RIRs using the image-source method [46]. The reverberation time is within the range of $[0.2, 0.6]$ s. Sensor noise was added with SNR = 15, 25, and 35 dB. Two microphone array geometries were used for training and validation, as depicted in Fig. 9. The first microphone array is an eight-element ULA with interelement spacing of 8 cm. The geometry of the second array is similar to that of the seven-element uniform circular array (UCA) used in the LibriCSS dataset [48] which has one microphone at the center and the other six uniformly distributed around a circle with a radius of 4.25 cm. The RIRs of rectangular rooms with randomly generated dimensions (length, width, and height) in the range of $[3 \times 3 \times 2.5, 7 \times 7 \times 3]$ m were simulated. The ULA was placed at 0.5 m from the wall, while the UCA was placed at the center of the room. Any two speakers were separated by at least 15° .

4.2 Implementation and evaluation metrics

In this study, the signal frame was 128 ms in length

with a stride of 32 ms. A 2048-point fast Fourier transform was used. The sample rate was 16 kHz. The feature vectors in (5) and (18) comprised $K = 257$ frequency bins in 1-3 kHz. In the experiment, SCnet and GLADnet are trained using the Adam optimizer with a learning rate of 0.001 and a gradient norm clipping of 3. The learning rate will be halved when the validation loss has no improvement for three consecutive epochs.

F1 score and confusion matrix are used to assess the speaker counting performance. PESQ [49] is employed as the metric for speech quality and is computed only in the period when the speech is present. In addition, we also evaluate the WER attained by the proposed system in comparison with the baselines, by using a transformer-based pretrained model from the SpeechBrain toolkit [57]. The pre-trained model was trained on the dataset of LibriSpeech. The WER obtained using this model when tested on *test-clean* subset is 1.9%.

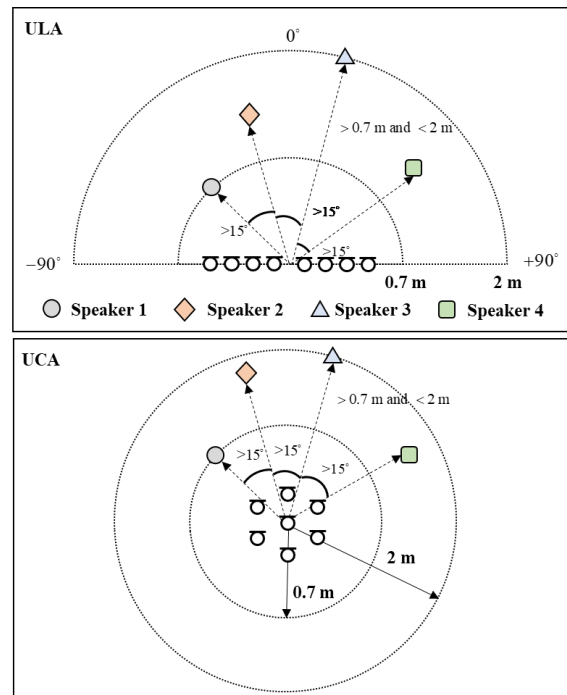


Figure 9 Settings for network training with different microphone array geometries.

Table 1 Comparison of speaker counting performance under different acoustical conditions in terms of F1 score

T60 (ms)	360			610			
SNR (dB)	30	20	10	30	20	10	Avg.
baseline 1	99.40	94.42	55.94	98.81	93.72	59.00	83.55
baseline 2	99.52	96.22	82.53	99.57	96.54	84.94	93.22
proposal 1	99.62	98.66	90.79	99.72	98.63	91.29	96.45
proposal 2	99.75	99.37	91.01	99.75	99.25	91.88	96.84

Table 2 Comparison of low-activity speaker counting performance under different acoustical conditions in terms of F1 score

T60 (ms)	360			610			
SNR (dB)	30	20	10	30	20	10	Avg.
baseline 1	91.34	89.49	54.31	92.50	84.92	50.73	77.22
baseline 2	97.65	85.91	64.27	96.29	86.47	65.78	82.73
proposal 1	99.70	95.58	71.17	99.16	94.41	74.47	89.08
proposal 2	99.70	98.43	78.21	99.75	98.10	80.22	92.40

4.3 Speaker counting performance

In the following, we examine several speaker counting methods for various levels of sensor noise and T60s. We generated 2000-sample speech mixtures for 1-4 speakers, with 0%, 10%, 20%, 30%, 40% overlap ratios, and dry speech signals from the *test-clean* subset of the LibriSpeech corpus. Sensor noise was added with SNR = 10, 20, and 30 dB. The measured RIRs were selected from the Multi-Channel Impulse Responses Database [47] recorded using an eight-element ULA with interelement spacing of 8 cm and T60 = 0.36, 0.61 s at Bar-Ilan University. The RIRs were measured in 15° intervals from -90° to 90° at distances of 1 and 2 m from the array center. Table I summarizes the speaker counting results in F1 scores. We compare the proposed counting approaches with two baselines. Baseline 1 is the method proposed in [33]. The SVM classifier with $\mathbf{f}_{\text{proposal 1}}$ in (7) as the input feature is used in the training. Baseline 2 is the SCnet trained with $\mathbf{f}_{\text{proposal 2}}$ in (22). For the proposed methods, proposals 1 and 2 represent the SCnet trained with $\mathbf{f}_{\text{proposal 1}}$ and $\mathbf{f}_{\text{proposal 2}}$ in (22). The speaker counting

performance summarized in Table I suggests that Baseline 1 performs comparably with Baseline 2 in high SNR conditions. However, the speaker counting performance of Baseline 1 degrades significantly as the SNR decreases. The features using the eigenvalues obtained from the spatial coherence matrix (proposals 1 and 2) considerably outperform those obtained from the spatial correlation matrix (baselines 1 and 2), especially when SNR is low. In addition, the method trained with the maximum similarity (proposal 2) could further improve the speaker counting performance over the method trained with eigenvalues only (proposal 1).

Next, we investigate speaker counting in low-activity scenarios using four-speaker mixtures, where the first speaker was active in only 5% duration. In Table II, we see significant performance degradation in the SCnet trained on the eigenvalues of the spatial correlation matrix (baselines 1 and 2), even in high-SNR conditions. By contrast, the SCnet trained on the eigenvalues and the maximum similarities computed using the proposed spatial coherence matrix (proposal 2) performs quite

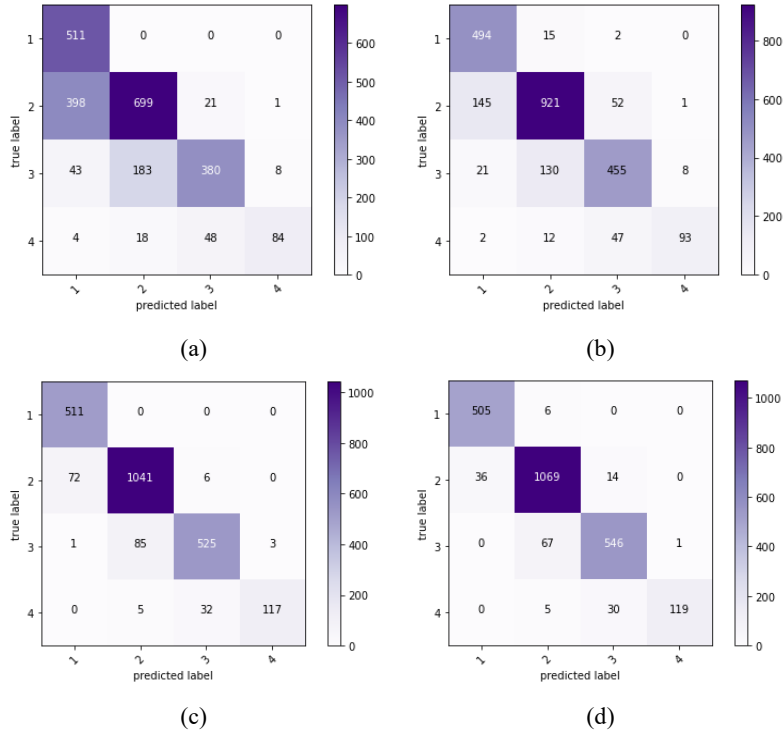


Figure 10 Confusion matrices for the speaker counting results obtained using (a) baseline 1, (b) baseline 2, (c) proposal 1, and (d) proposal 2.

satisfactorily despite the imbalanced activity of speakers.

Lastly, we examine speaker counting using the real-life recordings from the LibriCSS dataset [48]. There were 10 one-hour sessions, including in each session six 10-min mini-sessions with different speaker overlap ratios (0S, 0L, 10%, 20%, 30%, and 40%). In the 0% case, 0S and 0L represent the signals with short and long silence periods, where inter-utterance silence lasts between 0.1-0.5s and 2.9-3.0s. The test data was pre-segmented into 12-second clips containing 1 to 4 speakers in each session. The speaker count of each audio clip was labeled by using the ground-truth information. The results of speaker counting are summarized in the confusion matrices depicted in Fig. 10. The F1 scores for the baselines 1 and 2, proposals 1 and 2 were 88.37%, 92.44%, 96.48%, and 97.36%. It can be observed from Fig. 9 that the methods trained on the feature from the spatial coherence matrix (proposals 1 and 2) outperform the methods trained on the features from the spatial correlation matrix (baselines 1 and 2). Figures 5(c) and (d) show that the methods trained on

maximum similarities (proposal 2) yield significantly lower underestimation rates than the methods trained on eigenvalues only (proposal 1). For the BSS problems, underestimation can undermine the subsequent separation, while overestimation is less critical. In summary, the SCnet trained on the eigenvalues and maximum similarities from the coherence matrix exhibits superior speaker counting capability as well as robustness to noise and low-activity speakers, which is highly desirable in real-world applications.

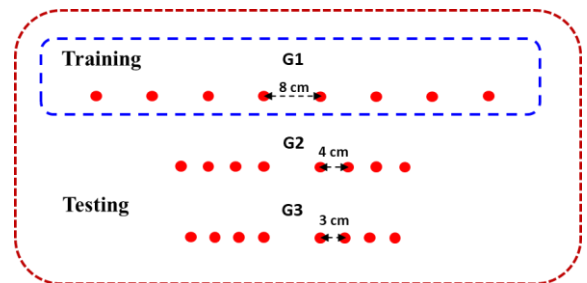


Figure 11 Microphone array settings for experiments to investigate the effects of array configurations.

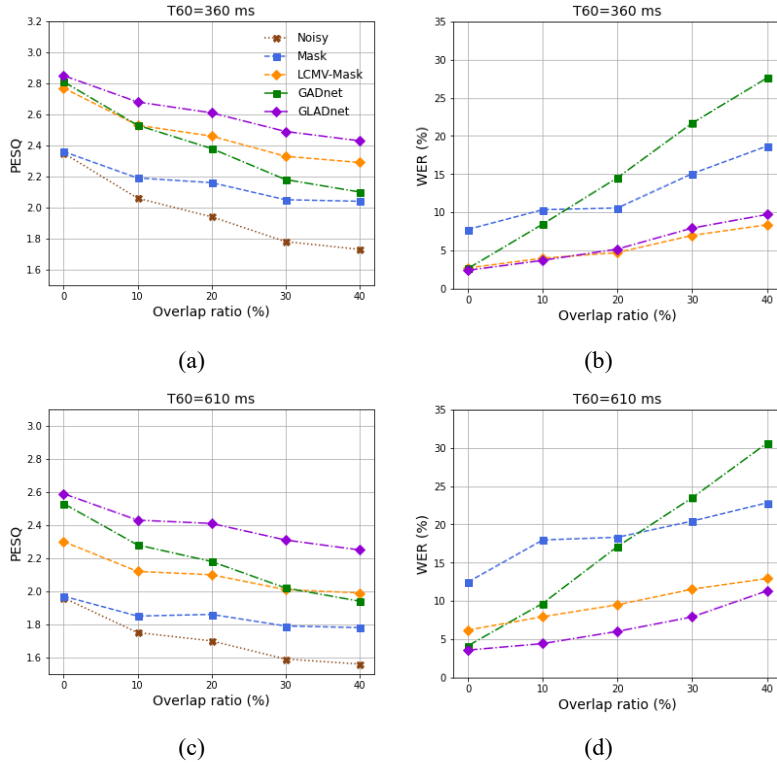


Figure 12 Comparison of separation performance in terms of (a), (c) PESQ and (b), (d) WER for different overlap ratios.

4.4 Speaker separation performance

In the following, we compare the proposed speaker separation approach (GLADnet) with three baselines. The first baseline (Mask) utilizes only a spectral mask (12). The second baseline (LCMV-Mask) is the simplex-based approach [33, 34] with beamforming and spectral masking (16). The third is the GLADnet trained on only the global activity, termed the global activity-driven network (GADnet). To assess the robustness of the proposed speaker separation approach when applied to unseen RIRs and array configurations, we created three 2000-sample test datasets for three different array configurations, using the measured RIRs from the Multi-Channel Impulse Responses Database [47]. As depicted in Fig. 11, the first array configuration (G1) is also in the training set, while the second and third array configurations (G2 and G3) are “unseen” to the trained model.

First, we examine the separation performance using the G1 configuration for various overlap ratios and T60s. The results in Fig. 12 show that the proposed GLADnet

outperforms the three baselines in terms of speech quality. The performance of the GADnet that is not trained with spatial features degraded drastically as the overlap ratio is increased. While the LCMV-Mask method attains comparable WER as GLADnet at moderate T60 = 360 ms, its separation performance drops sharply at high reverberation.

Next, the effect of array configurations on separation performance is investigated. Figure 13 reveals that the speech quality (PESQ) and the ASR performance (WER) using the LCMV-Mask method degrade as the array spacing and the array aperture are decreased, even for moderate T60’s. In contrast, the proposed GLADnet performs quite satisfactorily despite the unseen RIRs and array geometries.

We also evaluated the proposed network in speaker separation using a more realistic LibriCSS dataset. The dataset generation for network testing was identical to that in the speaker counting. Figure 14 shows that the LCMV-Mask method has a comparable performance with the proposed GLADnet when the overlap ratio is

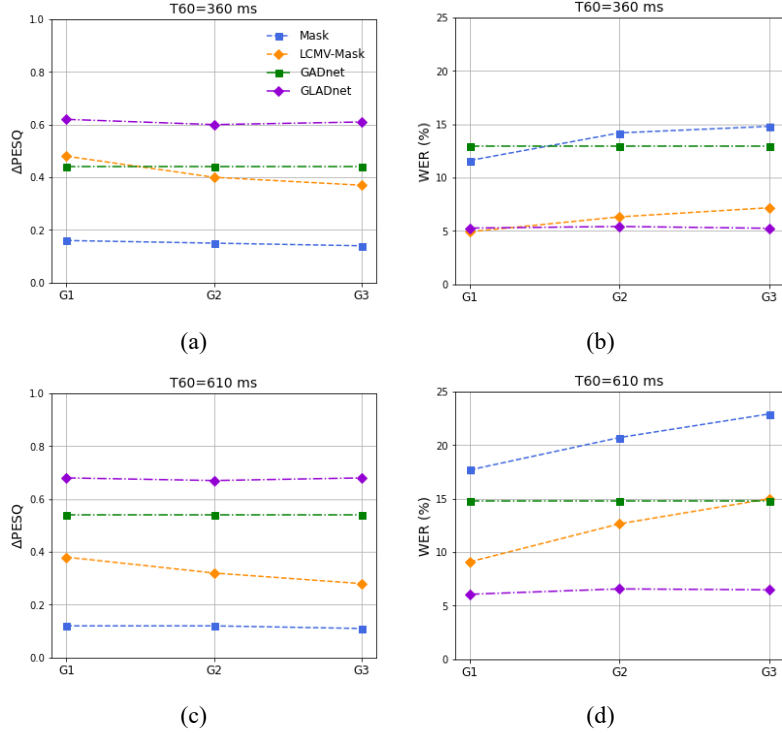


Figure 13 Comparison of separation performance in terms of (a), (c) PESQ and (b), (d) WER for different array configurations.

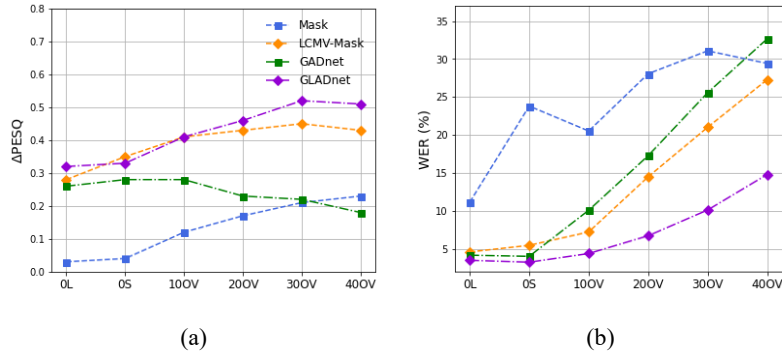


Figure 14 Comparison of separation performance in terms of (a) PESQ and (b) WER for the LibriCSS dataset.

low. However, the performance of LCMV-Mask drops drastically for high overlap ratios. In addition, GADnet performs satisfactorily only for non-overlapping speech mixtures. In summary, the proposed GLADnet which exploits the global and local activities of speakers outperforms the baselines with robustness to unseen RIRs, overlap ratios, and array configurations.

5 Conclusions

In this paper, a learning-based robust speaker counting

and separation system has been implemented by integrating array signal processing and DNN. In feature extraction, the spatial coherence matrix computed with wRTFs across time frames is adopted to effectively capture the spatial information of independent speakers. In speaker counting, the SCnet trained on the eigenvalues of the spatial coherence matrix and the maximum similarities between the global activity distribution of two speakers over time frames is conducive to intelligent speaker counting in adverse acoustic conditions,

especially in imbalanced voice activity scenarios. In speaker separation, the GLADnet based on global and local spatial activities proves capable of effective and robust enhancement and ASR with various overlap ratios for unseen RIRs and array configurations, which is highly desirable for real-world applications.

References

1. Vincent, E., Virtanen T., and Gannot, S.: Audio Source Separation and Speech Enhancement. (Wiley, NJ, USA, 2018)
2. Kawamoto, M., Matsuoka, K., and Ohnishi, N.: A method of blind separation for convolved nonstationary signals. *Neurocomputing* **22**, 157–171 (1998)
3. Buchner, H., Aichner, R., and Kellermann, W.: A generalization of blind source separation algorithms for convolutive mixtures based on second-order statistics. *IEEE Transactions on Audio, Speech and Language Processing* **13**(1), 120–134 (2005)
4. Koldovsky, Z. and Tichavsky, P.: Time-domain blind separation of audio sources on the basis of a complete ICA decomposition of an observation space. *IEEE Transactions on Audio, Speech and Language Processing* **19**(2), 406–416 (2011).
5. Kim, T., Eltoft, T., and Lee, T.-W.: Independent vector analysis: An extension of ICA to multivariate components. In: *International Conference on Independent Component Analysis and Signal Separation*. pp. 165–172 (2006)
6. Virtanen, T.: Monaural sound source separation by nonnegative matrix factorization with temporal continuity and sparseness criteria. *IEEE Transactions on Audio, Speech and Language Processing* **15**(3), 1066–1074 (2007)
7. Dikmen, O. and Cemgil, A.T.: Unsupervised single-channel source separation using Bayesian NMF. In: *Proc. of IEEE Workshop on Applications of Signal Processing to Audio and Acoustics (WASPAA)*, pp. 93–96 (2009)
8. Ozerov, A. and Fvotte, C.: Multichannel nonnegative matrix factorization in convolutive mixtures for audio source separation. *IEEE Transactions on Audio, Speech and Language Processing* **18**(3), 550–563 (2010).
9. Mitsufuji, Y. and Roebel, A.: Sound source separation based on non-negative tensor factorization incorporating spatial cue as prior knowledge. In: *Proc. of IEEE International Conference on Acoustics, Speech and Signal Processing (ICASSP)*, pp. 71–75 (2013)
10. Hershey, J. R., Chen, Z., Le Roux, J., and Watanabe, S.: Deep clustering: discriminative embeddings for segmentation and separation. In: *Proc. of IEEE International Conference on Acoustics, Speech and Signal Processing (ICASSP)*, pp. 31–35 (2016)
11. Chen, Z., Luo, Y., and Mesgarani, N.: Deep attractor network for single-microphone speaker separation. In: *Proc. of IEEE International Conference on Acoustics, Speech and Signal Processing (ICASSP)*, pp. 246–250 (2017)
12. Luo, Y. and Mesgarani, N.: Conv-TasNet: surpassing ideal time-frequency magnitude masking for speech separation. *IEEE Transactions on Audio, Speech and Language Processing* **27**(8), 1256–1266, (2019)
13. Lue, Y., Chen, Z., and Yoshioka, T.: Dual-path RNN: Efficient long sequence modeling for time-domain single-channel speech separation. In: *Proc. of IEEE International Conference on Acoustics, Speech and Signal Processing (ICASSP)*, pp. 46–50 (2020)
14. Yu, D., Kolbæk, M., Tan, Z., and Jensen, J.: Permutation invariant training of deep models for speaker-independent multi-talker speech separation. In: *Proc. of IEEE International Conference on Acoustics, Speech and Signal Processing (ICASSP)*, pp. 241–245 (2017)
15. Kolbæk, M., Yu, D., Tan, Z., and Jensen, J.: Multi-talker speech separation with utterance-level permutation invariant training of deep recurrent neural networks. *IEEE/ACM Transactions on Audio, Speech and Language Processing* **25**(10), 1901–1913, (2017)
16. Drude, L. and Haeb-Umbach, R.: Tight integration of spatial and spectral features for BSS with deep clustering embeddings. In: *Interspeech*, pp. 2650–2654 (2017)
17. Wang, Z.Q., Le Roux, J., and Hershey, J.R.: Multi-channel deep clustering: Discriminative spectral and spatial embeddings for speaker-independent speech separation. In: *Proc. of IEEE International Conference on Acoustics, Speech and Signal Processing (ICASSP)*, pp. 1–5 (2018)
18. Wang, Z. and Wang, D.: Combining spectral and spatial features for deep learning based blind speaker separation. *IEEE/ACM Transactions on Audio, Speech and Language Processing* **27**(2), 457–468 (2019)
19. Luo, Y., Han, C., Mesgarani, N., Ceolini, E., and Liu, S.: FaSNet: Low-latency adaptive beamforming for multi-microphone audio processing. In: *Proc. of IEEE Workshop Automatic Speech Recognition and Understanding*, pp. 260–267, (2019)
20. Kinoshita, K., Delcroix, M., Araki, S., and Nakatani, T.: Tackling real noisy reverberant meetings with all-neural source separation, counting, and diarization system. In: *Proc. of IEEE International Conference on Acoustics, Speech and Signal Processing (ICASSP)*, pp. 381–385 (2020)
21. Kolbak, M., Yu, D., Tan, Z., and Jensen, J.: Multitalker speech separation with utterance-level permutation invariant training of deep recurrent neural networks. *IEEE/ACM Transactions on Audio, Speech and Language Processing* **25**(10), 1901–1913 (2017)
22. Liu, Y. and Wang, D.: Divide and conquer: A deep CASA approach to talker-independent monaural speaker separation. *IEEE/ACM Transactions on Audio, Speech and Language*

- Processing 27(12), 2092–2102 (2019)
23. Nachmani, E., Adi, Y., and Wolf, L.: Voice separation with an unknown number of multiple speakers. In: International Conference on Machine Learning (ICML), pp. 2623–2634 (2020)
 24. Luo, Y. and Mesgarani, N.: Separating varying numbers of sources with auxiliary autoencoding loss. In: Interspeech (2020)
 25. Kinoshita, K., Drude, L., Delcroix, M., and Nakatani, T.: Listening to each speaker one by one with recurrent selective hearing networks. In: Proc. of IEEE International Conference on Acoustics, Speech and Signal Processing (ICASSP), pp. 5064–5068 (2018)
 26. Neumann, T., Kinoshita, K., Delcroix, M., Araki, S., Nakatani, T., and Haeb-Umbach, R.: All-neural online source separation counting and diarization for meeting analysis. In: Proc. of IEEE International Conference on Acoustics, Speech and Signal Processing (ICASSP), pp. 91–95 (2019)
 27. Jin, Z., Hao, X., and Su, X.: Coarse-to-fine recursive speech separation for unknown number of speakers. arXiv:2203.16054 (2022)
 28. Zhu, J., Yeh, R.A., and Hasegawa-Johnson M.: Multi-decoder dprnn: Source separation for variable number of speakers. In: Proc. of IEEE International Conference on Acoustics, Speech and Signal Processing (ICASSP), pp. 3420–3424 (2021)
 29. Wang, Z.-Q. and Wang, D.: Count and separate: Incorporating speaker counting for continuous speaker separation. In: Proc. of IEEE International Conference on Acoustics, Speech and Signal Processing (ICASSP), pp. 11–15 (2021)
 30. Higuchi, T., Kinoshita, K., Delcroix, M., Zmolikova, K., and Nakatani, T.: Deep Clustering-Based Beamforming for Separation with Unknown Number of Sources. In: Interspeech (2017)
 31. Chazan, S.E., Goldberger, J., and Gannot, S.: DNN-based concurrent speakers detector and its application to speaker extraction with LCMV beamforming. In: Proc. of IEEE International Conference on Acoustics, Speech and Signal Processing (ICASSP), pp. 6712–6716 (2018)
 32. Chazan, S.E., Gannot, S., and Goldberger, J.: Attention-based neural network for joint diarization and speaker extraction. In: Proc. of IEEE International Workshop on Acoustic Signal Enhancement (IWAENC), pp. 301–305 (2018)
 33. Laufer-Goldshtein, B., Talmon, R., and Gannot, S.: Global and local simplex representations for multichannel source separation. IEEE/ACM Transactions on Audio, Speech and Language Processing 28(1), 914–928 (2020)
 34. Laufer-Goldshtein, B., Talmon, R., and Gannot, S.: Audio source separation by activity probability detection with maximum correlation and simplex geometry. EURASIP Journal on Audio, Speech, and Music Processing, 2021, 5 (2021)
 35. Ephrat, A., Mosseri, I., Lang, O., Dekel, T., Wilson, K., Hassidim, A., Freeman, W.T., and Rubinstein, M.: Looking to listen at the cocktail party: A speaker-independent audio-visual model for speech separation. ACM Transactions on Graphics. 37(4), 1–11 (2018)
 36. Li, C. and Qian, Y.: Listen, watch and understand at the cocktail party: Audio-visual-contextual speech separation. In: Interspeech, pp. 1426–1430 (2020)
 37. Žmolíková, K., Delcroix, M., Kinoshita, K., Ochiai, T., Nakatani, T., Burget, L., and Černocký, J.: Speakerbeam: Speaker aware neural network for target speaker extraction in speech mixtures. IEEE Journal of Selected Topics in Signal Processing 13(4), 800–814, (2019)
 38. Wang, Q., Muckenhirn, H., Wilson, K., Sridhar, P., Wu, Z., Hershey, J.R., Saurous, R.A., Weiss, R.J., Jia, Y., and Moreno, I.L.: VoiceFilter: Targeted Voice Separation by Speaker-Conditioned Spectrogram Masking. In: Interspeech, pp. 2728–2732 (2019)
 39. Ge, M., Xu, C., Wang, L., Chang, E.S., Dang, J., and Li, H.: Spex+: A complete time domain speaker extraction network. In: Interspeech, pp. 1406–1410 (2020)
 40. Gu, R., Chen, L., Zhang, S.-X., Zheng, J., Xu, Y., Yu, M., Su, D., Zou, Y., and Yu, D.: Neural spatial filter: Target speaker speech separation assisted with directional information. In: Interspeech, pp. 4290–4294 (2019)
 41. Delcroix, M., Ochiai, T., Zmolikova, K., Kinoshita, K., Tawara, N., Nakatani, T., and Araki, S.: Improving speaker discrimination of target speech extraction with time-domain speakerbeam. In: Proc. of IEEE International Conference on Acoustics, Speech and Signal Processing (ICASSP), pp. 691–695 (2020)
 42. Han, J., Rao, W., Wang, Y., and Long, Y.: Improving channel decorrelation for multi-channel target speech extraction. In: Proc. of IEEE International Conference on Acoustics, Speech and Signal Processing (ICASSP), pp. 6094–6098 (2021)
 43. Hsu, Y., Lee, Y., and Bai, M.R.: Learning-based personal speech enhancement for teleconferencing by exploiting spatial-spectral features. In: Proc. of IEEE International Conference on Acoustics, Speech and Signal Processing (ICASSP), pp. 8787–8791 (2022)
 44. Delcroix, M., Zmol'iková, K., Ochiai, T., Kinoshita, K., and Nakatani, T.: Speaker activity driven neural speech extraction. In: Proc. of IEEE International Conference on Acoustics, Speech and Signal Processing (ICASSP), pp. 6099–6103 (2021)
 45. Laufer-Goldshtein, B., Talmon, R., and Gannot, S.: Source counting and separation based on simplex analysis. IEEE/ACM Transactions on Audio, Speech and Language Processing 66(24) 6458–6473 (2018)
 46. Lehmann, E. and Johansson, A.: Prediction of energy decay in room impulse responses simulated with an image-source model. The Journal of the Acoustical Society of America. 124(1), pp. 269–277 (2008)
 47. Hadad, E., Heese, F., Vary, P., and Gannot, S.: Multichannel audio database in various acoustic environments. In: Proc. of IEEE International Workshop on Acoustic Signal Enhancement

- (IWAENC), pp. 313–317 (2014)
48. Chen, Z., Yoshioka, T., Lu, L., Zhou, T., Meng, Z., Luo, Y., Wu, J., and Li, J.: Continuous speech separation: Dataset and analysis. In: Proc. of IEEE International Conference on Acoustics, Speech and Signal Processing (ICASSP), pp. 7484–7288 (2020)
 49. Rix, A.W., Beerends, J.G., Hollier, M.P., and Hekstra, A.P.: Perceptual evaluation of speech quality (PESQ)-a new method for speech quality assessment of telephone networks and codecs. In: Proc. of IEEE International Conference on Acoustics, Speech and Signal Processing (ICASSP), pp. 749–752 (2021)
 50. Yilmaz, O. and Rickard, S.: Blind separation of speech mixtures via time-frequency masking. *IEEE Transactions on Signal Processing* **52**(7), 1830–1847, (2004)
 51. Gannot, S., Burshtein, D., and Weinstein, E.: Signal enhancement using beamforming and nonstationarity with applications to speech. *IEEE Transactions on Signal Processing* **49**(8) 1614–1626, (2001)
 52. Ma, W.-K. et al.: A signal processing perspective on hyperspectral unmixing: Insights from remote sensing. *IEEE Signal Processing Magazine* **31**(1), pp. 67–81 (2014)
 53. Scharnhorst, K.: Angles in complex vector spaces. *Acta Applicandae Mathematicae*. 69(1), 95–103 (2001)
 54. Çetin, O. and Shriberg, E.: Analysis of overlaps in meetings by dialog factors hot spots speakers and collection site: insights for automatic speech recognition. In: *Interspeech*, pp. 293–296, (2006)
 55. Tan, K. and Wang, D.: A convolutional recurrent neural network for real-time speech enhancement. In: *Interspeech*, pp. 3229–3233 (2018)
 56. Panayotov, V., Chen, G., Povey, D., and Khudanpur, S.: Librispeech: an ASR corpus based on public domain audio books. In: Proc. of IEEE International Conference on Acoustics, Speech and Signal Processing (ICASSP), pp. 5206–5210 (2015)
 57. Ravanelli, M. et al.: SpeechBrain: A general-purpose speech toolkit. *arXiv preprint arXiv:2106.04624* (2021)